

Distribution of Chromosome 18 and X Centric Heterochromatin in the Interphase Nucleus of Cultured Human Cells

SUSANNE POPP,^{*1} HANS PETER SCHOLL,^{*} PETER LOOS,[†] ANNA JAUCH,^{*} ERNST STELZER,[‡]
CHRISTOPH CREMER,[†] AND THOMAS CREMER^{*}

^{*}Institute of Human Genetics and Anthropology, University of Heidelberg, INF 328, D-6900 Heidelberg, Federal Republic of Germany;

[†]Institute of Applied Physics I, University of Heidelberg, Albert-Überle-Str. 3-5, D-6900 Heidelberg, Federal Republic of Germany;

and [‡]European Molecular Biology Laboratory (EMBL), Meyerhofstr. 1, D-6900 Heidelberg, Federal Republic of Germany

In situ hybridization of human chromosome 18 and X-specific alphoid DNA-probes was performed in combination with three dimensional (3D) and two dimensional (2D) image analysis to study the interphase distribution of the centric heterochromatin (18c and Xc) of these chromosomes in cultured human cells. 3D analyses of 18c targets using confocal laser scanning microscopy indicated a nonrandom disposition in 73 amniotic fluid cell nuclei. The shape of these nuclei resembled rather flat cylinders or ellipsoids and targets were preferentially arranged in a domain around the nuclear center, but close to or associated with the nuclear envelope. Within this domain, however, positionings of the two targets occurred independently from each other, i.e., the two targets were observed with similar frequencies at the same (upper or lower) side of the nuclear envelope as those on opposite sides. This result strongly argues against any permanent homologous association of 18c. A 2D analytical approach was used for the rapid evaluation of 18c positions in over 4000 interphase nuclei from normal male and female individuals, as well as individuals with trisomy 18 and Bloom's syndrome. In addition to epithelially derived amniotic fluid cells, investigated cell types included *in vitro* cultivated fibroblastoid cells established from fetal lung tissue and skin-derived fibroblasts. In agreement with the above 3D observations 18c targets were found significantly closer ($P < 0.01$) to the center of the 2D nuclear image (CNI) and to each other in all these cultures compared to a random distribution derived from corresponding ellipsoid or cylinder model nuclei. For comparison, a chromosome X-specific alphoid DNA probe was used to investigate the 2D distribution of chromosome X centric heterochromatin in the same cell types. Two dimensional Xc-Xc and Xc-CNI distances fit a random distribution in diploid normal and Bloom's syndrome nuclei, as well as in nuclei with trisomy X. The different distributions of 18c and Xc targets were confirmed by the simultaneous staining of these targets in different colors within individual nuclei using a double *in situ* hybridization approach. © 1990 Academic Press, Inc.

INTRODUCTION

Chromosomes occupy distinct territories within the nucleus of all animal and plant species studied so far [1-7]. To what if any extent the three-dimensional (3D) organization of individual interphase chromosome domains and their suprachromosomal arrangements may be functionally important presents an unresolved puzzle (for review see Refs. [8-12]). Some investigations have indicated that chromatin arrangements may be cell type-dependent and change during differentiation or under pathophysiological conditions [13-18]. In contrast, Mathog and Sedat [6] in a recent study of the 3D organization of polytene nuclei in *Drosophila melanogaster* salivary glands have concluded that chromosome position in the polytene nucleus does not play a major role in the normal genetic regulation of euchromatic loci.

Until recently, appropriate methods were not available to resolve these questions unambiguously. This situation may now rapidly change as a result of recent advances in two fields, namely, 3D digital imaging microscopy ([19-21]; for a methodological review see Ref. [22]) and the selective visualization of chromosomes directly in the cell nucleus by *in situ* hybridization of chromosome-specific DNA probes [4, 23-30].

In a previous study [30] we have used double *in situ* hybridization in combination with a 2D image analysis approach to investigate the distribution of the centric heterochromatin of chromosome 15 and of the heterochromatic region 1q12 in interphase nuclei of cultured human cells. In comparison with the 3D evaluation of nuclei (see below) this 2D approach has the advantage that large numbers of nuclei can be rapidly evaluated to detect significant deviations from a random target distribution. In three human diploid cell types studied, including human lymphocytes, amniotic fluid cells, and fibroblasts, the labeled segments of the two chromo-

¹ To whom reprint requests should be addressed at Institut für Humangenetik und Anthropologie, Universität Heidelberg, Im Neuenheimer Feld 328, D-6900 Heidelberg, Federal Republic of Germany.

somes 15 were distributed significantly closer to the center of the 2D nuclear image and to each other than the labeled chromosome 1 segments. This result could be explained by the association of the chromosome 15 nucleolus organizer regions (NOR) with the more centrally located nucleoli. The labeled segments of both chromosomes, however, showed a pronounced internuclear variability in their relative positioning, rejecting the idea of any strict and permanent association of the labeled homologous or nonhomologous targets.

In the present study we have combined 2D analyses with a 3D analytical approach to interphase chromosome topography based on *in situ* hybridization and confocal scanning laser microscopy (CSLM) [31–33]. For the following reasons two alphoid DNA probes were chosen, which under appropriate conditions of stringency hybridize specifically to the centric heterochromatin of chromosomes 18 or X [34–36]. Previous analyses of the chromosome disposition in human metaphase spreads have consistently shown that smaller chromosomes were distributed closer to the center of the metaphase spread than larger ones [38, 39]. The comparison of the interphase distribution of a smaller human chromosome, such as chromosome 18, with a larger one, such as the active X chromosome, should indicate whether size-dependent differences in the distribution of metaphase chromosomes are also apparent in interphase nuclei of cultured human cells. A relationship between the interphase and metaphase distributions of chromosomes has been suggested by laser-uv-microbeam experiments ([40]; H. Baumann and T. Cremer, unpublished data). For example, microirradiation of either the center or the periphery of elliptically shaped interphase nuclei of cultured Chinese hamster fibroblastoid cells has shown that the relative positions of microirradiated chromatin sites were still maintained to a significant extent during the subsequent cell cycle and in the following metaphase [41]. Since chromosome 18 does not contain a NOR, the hypothetical size-dependent difference in the interphase distribution of this chromosome compared to that of larger ones would demand a different explanation than the results of our previous experiments on the distribution of 15c and 1q12. The peripheral localization of the Barr body representing the inactive X chromosome in female nuclei has been reported for some but not all cell types investigated so far [37]. In contrast, the interphase distribution of the active X has not been studied in detail [34].

The present study was carried out to answer three questions: (1) Are the results obtained by the 2D and 3D approach after various cell fixation procedures consistent with each other? (2) Are the interphase positions of chromosome 18 and the (active) X chromosome significantly different in accordance with the above hypothesis of a chromosome size-dependent distribution? (3) If so, can the same deviation of a given chromosome from random model distributions be found consistently in vari-

ous types of cultured human cells or can differences be observed depending on the source of the material and a normal or aberrant karyotype?

The 3D distribution of the 18c target was investigated in detail by optical serial sections of 73 amniotic fluid cell nuclei using CSLM. For comparison, single and double *in situ* hybridizations were applied in combination with our 2D image analysis approach [30] to compare the interphase distribution of 18c and Xc targets in over 4000 cells cultured *in vitro* from various tissues of normal diploid, male and female individuals, as well as from a female with trisomy X, a male patient with trisomy 18, and two patients with Bloom's syndrome. As a control, the known peripheral distribution of inactive X chromosomes in fibroblast nuclei [37] was studied in Feulgen-stained cells with trisomy X.

MATERIALS AND METHODS

Cell Material

Amniotic fluid cells (46, XY, and 46, XX) were obtained in the 17th week of pregnancy by diagnostic amniocentesis (courtesy of Dr. Werner Schmidt, University of Heidelberg). These cells show a fibroblastoid-like growth pattern (F-type) although expression of prekeratin points to their epithelial origin [42]. Primary amniotic fluid cell cultures were used directly or after one subcultivation (see below) for *in situ* hybridization experiments. Fibroblastoid cells derived from lung tissue of a male fetus (46, XY) were commercially obtained (Flow 2000, Flow Laboratories). Skin-derived fibroblast cultures from male and female patients with Bloom's syndrome (EN-1C and GM 1492) were provided by Dr. H. W. Rüdiger (University of Hamburg). Fibroblast cultures with 47, XY + 18, and 47, XXX, respectively, were established by Dr. H. D. Hager (University of Heidelberg) from fetal skin after induced abortion requested by the parents. These cultures were used for *in situ* hybridization experiments during phase II of their replicative lifespans [43].

Cells were grown in F10 medium supplemented with 10–20% FCS, 0.5% L-glutamine, 10 IU/ml penicillin and 10 μ g/ml streptomycin at 37°C in a humidified incubator with 5% CO₂. Slides with fixed cells were obtained by the following protocols: (a) Cell cultures were detached by a brief treatment with 0.05% trypsin and 0.02% EDTA, seeded on glass slides, further grown for 24–48 h, fixed three times (5–10 min each) with ice-cold methanol/acetic acid (3/1, v/v), air dried, and stored at 4°C in 70% ethanol (up to 4 months) until use. (b) Detached cells were directly fixed with methanol/acetic acid in suspension, dropped on slides, and further treated as described above. (c) Cell cultures were treated with colcemid (0.2 μ g/ml) for 2 h, detached by trypsin-EDTA, further treated with a hypotonic shock (0.0375 M KCl for 25 min at 37°C), fixed, and air dried. Pretreatments a–c were used for *in situ* hybridization experiments in combination with 2D image analysis. (d) For 3D experiments it was essential to maintain the 3D-structure of the nuclei. Air drying was therefore carefully avoided during all fixation and *in situ* hybridization steps. Male and female amniotic fluid cells grown on slides were briefly washed with phosphate-buffered saline (PBS: 140 mM NaCl, 2.7 mM KCl, 1.5 mM KH₂PO₄, 6.5 mM Na₂HPO₄; pH 7.0), fixed with 4% paraformaldehyde in PBS for 5 min, again washed in PBS, exposed two times to 0.1% triton-saponin in PBS for 5 min each, washed in 0.1 M Tris-HCl (pH 7.2) for 2 min, equilibrated in 20% glycerol in PBS for 20 min, freeze-thawed three times by briefly dipping in liquid nitrogen, and stored at 4°C in PBS containing 0.04% sodium azide until use. (e) For Feulgen staining, cells were fixed as described in d, except that cells were air dried.

DNA Probes and Labeling Procedures

The probes pXBR and L1.84 represent tandemly repeated alphoid sequences organized predominantly at the pericentromeric region of either the X chromosome (pXBR) or chromosome 18 (L1.84) [44–46]. Plasmid DNAs containing the respective inserts were either nick-translated with [³H]dTTP [24] or with biotin-11-dUTP [47] or mercurolyzed by incubation with mercury acetate [48].

In situ Hybridization and Detection of DNA Probes

Single and double *in situ* hybridizations of the alphoid DNA probes were performed as described [24, 36]. Hybridization conditions and posthybridization washes were chosen which favored strong hybridization signals at the pericentromeric heterochromatin of either the X or 18 chromosome, while crosshybridization to related sequences in the constitutive heterochromatin of other chromosomes was negligible [35, 36]. Detection of ³H-labeled probes was achieved by autoradiography. For 2D studies, chemically modified probes were visualized with an alkaline phosphatase or peroxidase reaction [30]. Nuclei were counterstained with Giemsa. For 3D studies, the biotinylated probe L1.84 was detected by indirect immunofluorescence using a rabbit anti-biotin IgG for the first step and a fluoresceine isothiocyanate (FITC)-conjugated second goat anti-rabbit IgG provided by ENZO, Neckargemünd, FRG [35]. After counterstaining of nuclei with propidium iodide, preparations were mounted in PBS/glycerol (1/9, v/v) containing 0.1% 1,4-phenylenediamine dihydrochloride as antifade (Serva, Heidelberg, FRG) [49].

Visualization of Barr Bodies

Feulgen staining [50] was applied to visualize the inactivated X chromosomes (Barr bodies) in fibroblasts from a female with trisomy X. For 2D distance measurements (see below) the center of each Barr body was arbitrarily defined as a reference point.

Evaluation of Nuclei

CSLM and 3D image analysis. The confocal beam scanning laser microscope (CBSLM) was designed and built at the EMBL [51]. The instrument was used in the epifluorescence set up with a NPL-Fluotar objective 100×/1.32 from Leitz. FITC and propidium iodide in the sample were excited with the 476.5-nm line of an argon ion laser (Spectra Physics 2016-04S). The filter combination consisted of a narrow band 476.5-nm interference filter, a Leitz 510-nm dichroic mirror, and a G530 longpass filter. This combination allowed the fluorescent light emitted by both fluorochromes (>530 nm) to enter the detector pinhole and the photomultiplier (PMT 1463-01; Hamamatsu Phototronics K.K., Hamamatsu City, Japan). A pinhole diameter of 50 μm was used, which is optimal for the CBSLM. Using the Raleigh criterion for a confocal setup the lateral (x, y) resolution was estimated to be about 200 nm. The measured vertical (z) resolution of the CBSLM expressed in terms of the fullwidth half-maximum of an intensity profile measured along the z-axis (for further explanation see Ref. [33]) was at the theoretical limit (approximately, 700 nm). Serial horizontal sections, i.e., sections parallel to the cell growth-supporting surface, were performed at a distance of 0.4 μm (±5%). The image size was 512 × 512 pixels. The height z of the nucleus was estimated from the number of these serial sections clearly containing nuclear material. An ellipse was fitted to the horizontal section with the largest nuclear area and used to measure the two lateral diameters x (smaller axis) and y (larger axis). The 3D center of each optically sectioned nucleus (referred to as CN) was operationally defined by the intersection of x and y. When a chromosomal target extended through several light optical sections, the center of the target from which distance measurements were undertaken was arbitrarily placed in the section with the largest lateral extension of the target or, if this lateral extension was rather uniform, in the middle of the sections comprising the target. In 73 horizontally sectioned nuclei the 3D coordinates of CN and of the two 18c targets were evaluated and used to calculate 3D target–target dis-

tances and 3D target–CN distances. From 14 of these nuclei the target-containing sections were drawn on plastic sheets attached to the TV screen, while in 59 nuclei each light-optical section was photographically recorded. These latter nuclei were also used to investigate the association of targets with the nuclear envelope. 3D distances were normalized by division with the maximum diameter of the adapted model nucleus (see below). In 36 cases vertical sections, i.e., sections perpendicular to the growth surface, were taken through nuclei at a level where these sections comprised a chromosome target region.

Transmission light microscopy and 2D image analysis. 2D image analysis of nuclei observed by transmission light microscopy was performed as previously described [30].

Model Calculations

For each 3D and 2D experiment, 10,000 ellipsoids and cylinders were simulated as model nuclei to calculate the random distribution of point-like chromosomal targets and to calculate model distribution functions of their normalized 3D or 2D distances. For 2D experiments model functions were calculated by orthogonal projection of random 3D distances onto the x,y-plane as described [30]. Model distribution functions of 3D distances were obtained with appropriate modifications. The diameters x, y, and z measured in each experimental nucleus were used to adapt both an ellipsoid and a flat cylinder of corresponding size. The fraction of model nuclei with given ratios of the x-, y-, and z-axes reflected the corresponding fraction of experimental nuclei.

Statistical Analyses

To test the fitting of the experimental and model curves, the Kolmogorov–Smirnov one-sample test was used [30, 52]. The Kolmogorov–Smirnov two-sample test [52] was chosen to test for significant differences between 18c and Xc distribution functions of distances. In an attempt to avoid the overinterpretation of small deviations, a biological reason for a nonrandom chromosome disposition was tentatively considered only if $P < 0.01$ was fulfilled for both the ellipsoid and the cylinder model in several independent experiments. On the other hand, failure to detect such a significant deviation would indicate a highly variable disposition of a chromosomal target, but should not be regarded as definitive proof for its completely random distribution (see Discussion).

RESULTS

After *in situ* hybridization with the 18c and Xc probes most nuclei in the evaluated cell samples showed the expected number of major hybridization signals, i.e., two 18c spots in nuclei of both sexes with a normal karyotype, one Xc spot in male diploid cells, two Xc spots in female diploid cells, and three spots in cells with trisomy 18 or X (for examples, see Figs. 1 and 5). Frequency distributions of spot numbers observed in normal and aberrant interphase nuclei after *in situ* hybridization with alphoid DNA probes have been reported in detail elsewhere [5, 35, 36]. From each slide, areas with satisfactory hybridization were chosen for further evaluation (range of nuclei with expected spot numbers 55–95%). Essentially the same results were obtained from samples at the upper and lower side of this range. Nuclei which showed high background or insufficient signal intensities or had shapes which could not conveniently be fitted by an ellipse were excluded as described previously [30]. Additional signals of clearly minor intensity were occa-

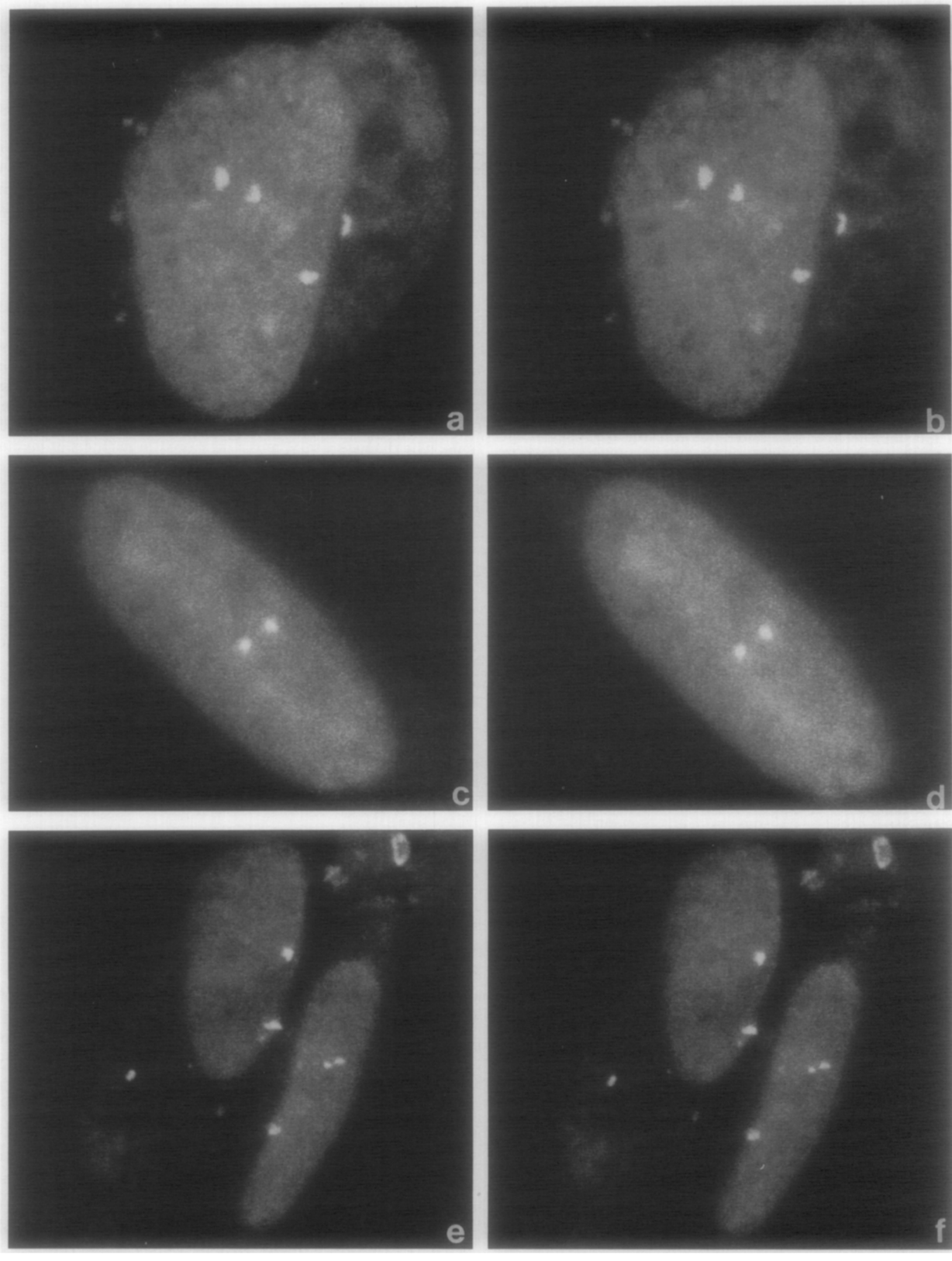


FIG. 1. Stereo pairs obtained with the CSLM from horizontally sectioned amniotic fluid cell nuclei after fluorescence *in situ* hybridization with the biotinylated probe L1.84. Nuclei were counterstained with propidium iodide. The procedure by which stereo pairs have been calculated is described in Rosa *et al.* [63]. (a, b) The two hybridization signals seen in the left of two overlapping nuclei are both associated with the upper

sionally seen due to crosshybridization of these aliphoid DNA probes to other chromosomes, but were also excluded from further consideration [30, 36].

3D Analyses of 18c Positions in Amniotic Fluid Cell Nuclei

Data obtained from male and female amniotic fluid cells were essentially the same and are therefore described together. Figure 1 presents typical stereo pairs obtained from horizontally sectioned nuclei by appropriate projection of some 20 optical sections per nucleus. Figure 2 shows examples of optical sections of nuclei performed perpendicularly to the growth surface and taken directly through labeled 18c regions. For further reference, the part of the nuclear envelope adjacent to the growth surface area (Fig. 2, bottom) is designated as lower nuclear envelope, while the opposite part which could be viewed directly from above in epifluorescence microscopy is referred to as upper nuclear envelope. In these vertical sections 18c targets with few exceptions appeared associated with either the upper (type a) or lower (type b) nuclear envelope (Figs. 2a and 2b). In only three of 36 *z*-axis scans were we unable to observe such an association (type c; Fig. 2c). The sensitivity of the present methods would not exclude the possibility of a few chromatin fibers extending from such a target to the nuclear envelope. In one vertically sectioned nucleus the fluorescent target appeared to be extended throughout the nucleus between the upper and lower nuclear envelope (type d; Fig. 2d). Note that each target appeared as a quite compact, although occasionally split spot (e.g., Fig. 1e), which was clearly elongated along the *z*-axis (Fig. 2). We consider this elongation as an artifact of the impaired *z*-axis resolution of the CSLM. Accordingly, targets which were close to the nuclear envelope may have appeared as if they had direct contact with it although in fact this may have not been the case (see also Discussion). On the other hand, the *z*-resolution (700 nm) is clearly sufficient in these nuclei (average height $4.2 \pm 1.0 \mu\text{m}$) to decide whether a target was localized in an upper or lower nuclear domain in close neighborhood to the envelope.

Similar frequencies of target types a–d were observed in vertically and horizontally sectioned nuclei (Table 1A). Table 1B shows the observed correlations of target types a–d in 59 horizontally sectioned nuclei. In 11 nuclei both 18c targets were associated with the upper nuclear envelope (aa). The same number was obtained

for nuclei in which both targets were associated with the lower part (bb), while 19 nuclei showed one 18c target associated with the upper nuclear envelope and the other target with the lower one (ab). These observed numbers for aa, bb, and ab cases do not significantly deviate from the numbers of nuclei expected in the case where both 18c targets were associated with the upper or lower nuclear envelope *independently* from each other.

Figure 3a shows measurements of 3D distances between each 18c target and the center of the nucleus (CN) (for definition see Materials and Methods) in 73 amniotic fluid cell nuclei. When compared with both the cylinder and the ellipsoid model, three-dimensional 18c–CN distances were significantly smaller than expected ($P < 0.01$). Accordingly, a significant deviation of three-dimensional 18c–18c distances from a random distribution should also be expected, but could not be demonstrated in the present 3D experiments (Fig. 3b). This discrepancy was possibly due to the smaller number of 18c–18c measurements, which was only half the number of measurements for 18c–CN distances.

The frequent association of 18c targets with opposite sites of the nuclear envelope as described above may at first glance appear in contradiction to the finding of significantly smaller 18c–CN distances (and smaller 18c–18c 2D distances, see below). A preferential localization at the outer rim of the nuclear image as seen in vertical sections (Figs. 2a and 2b), however, should not be confused with a preferential localization at the outer nuclear rim seen in horizontal sections. The latter distribution is typical for Barr bodies (see below, Fig. 5c) in clear contrast to 18c targets. The apparent contradiction is resolved if one takes into account that the typical 3D configuration of the nuclei evaluated in this study is not a sphere but resembles an ellipsoid or a flat cylinder (mean axis ratio 0.6 ± 0.1 for *x/y* and 0.25 ± 0.1 for *z/x*). Accordingly, 18c–CNI distances are largely dependent on the actual distribution of the target. Taken together the results of the above 3D analyses indicate that the 18c targets were preferentially located in a domain both near to the nuclear center and close to/associated with the nuclear envelope.

2D Analyses of 18c and Xc Positions in Human Interphase Nuclei

For 2D analyses double and single *in situ* hybridization experiments were performed with the 18c and Xc probes in various cell types. Measurements included 2D

part of the nuclear envelope, while the two hybridization signals contained in the right nucleus are associated with opposite parts of the envelope (field size $24.5 \times 23.5 \mu\text{m}$, eight averages per image, 19 sections, step size $0.4 \mu\text{m}$). (c, d) Both hybridization signals are located within the same serial sections and associated with the upper nuclear envelope (field size $26 \times 21 \mu\text{m}$, eight averages per image, 16 sections, step size $0.4 \mu\text{m}$). (e, f) In each of the two nuclei the two hybridization signals are associated with opposite parts of the nuclear envelope. Accordingly, 3D target–target distances are considerably larger than those in the examples shown above (field size $39 \times 35 \mu\text{m}$, eight averages per image, 18 sections, step size $0.4 \mu\text{m}$). One hybridization signal in the right nucleus is clearly split. It is not yet clear whether the splitting of a target depends on the state of its replication during the cell cycle or on other factors [36].

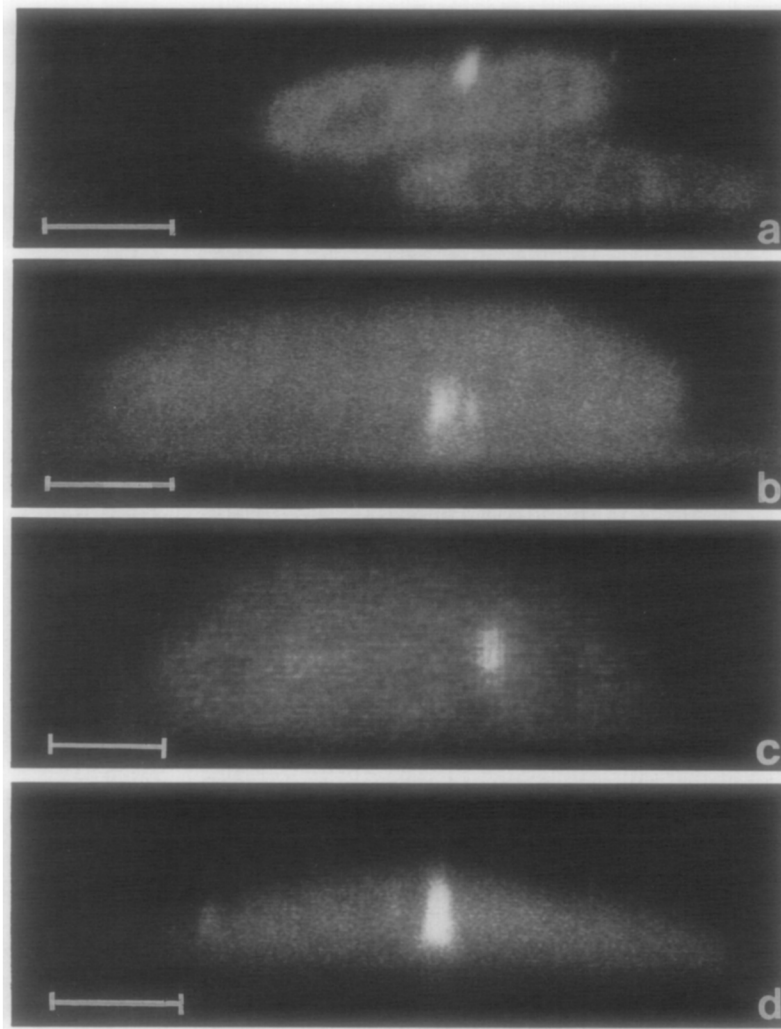


FIG. 2. Vertical optical sections (x -, z -views) performed with the CSLM through five amniotic fluid cell nuclei after fluorescence *in situ* hybridization with probe L1.84. Bar represents $5\ \mu\text{m}$. (a) Two overlapping nuclei are sectioned (compare Figs. 1a and 1b). In the above nucleus an 18c target is associated with the upper nuclear envelope (target type a; eight averages per image, total thickness of both the upper and the lower nucleus $4\ \mu\text{m}$). (b) 18c is associated with the lower nuclear envelope (target type b; eight averages per image, total thickness of the nucleus is $7.5\ \mu\text{m}$). (c) 18c is not associated with the nuclear envelope (target type c; 10 averages per image, total thickness of the nucleus is $9\ \mu\text{m}$). (d) 18c is extended throughout the nucleus and associated with both the upper and the lower part of the nuclear envelope (target type d; eight averages per image, total thickness of the nucleus is $4\ \mu\text{m}$).

distances between each target site (18c or Xc) and the center of the nuclear image (CNI), 2D distances between homologous targets (18c–18c or Xc–Xc), and in the case of double *in situ* hybridization also 2D distances between nonhomologous targets (18c–Xc).

Three double *in situ* hybridization experiments were performed (Table 2, Nos. 3, 4, and 8). As an example, Fig. 4 shows the results of Experiment 4 performed with amniotic fluid cells from a male fetus with 46, XY. Both 18c–CNI (Fig. 4a, black triangles) and 18c–18c 2D distances (Fig. 4b) showed a significant predominance of smaller distances. In contrast, Xc–CNI (Fig. 4a, white triangles) and Xc–18c 2D distances (Fig. 4c) fit the ex-

pectation of a random model distribution. The same result was observed in Experiment 8 carried out with lung-derived male fibroblastoid cells. In the third experiment, however, performed with normal diploid female amniotic fluid cells (Table 2, No. 3), both the 18c and Xc sites were distributed significantly closer to each other and the center of the nuclear image.

In four single hybridization experiments with probe pXBR, Xc–Xc and Xc–CNI 2D distances again fit the random model distribution. In addition to normal diploid cells (Table 2, Nos. 5 and 6), these experiments included Bloom's syndrome nuclei (Table 2, No. 11) and nuclei with trisomy X (Table 2, No. 14; Fig. 5b). Fibro-

TABLE 1A

Relationship of 18c Targets with the Nuclear Envelope in 3D-Reconstructed Amniotic Fluid Cell Nuclei

	<i>n</i> ^a	18c target type			
		<i>a</i>	<i>b</i>	<i>c</i>	<i>d</i>
Vertically sectioned nuclei (see Fig. 2)	36	16 (44.4%)	16 (44.4%)	3 (8.3%)	1 (2.8%)
Horizontally sectioned nuclei	118	46 (39.0%)	46 (39.0%)	9 (7.6%)	17 ^b (14.4%)

Note. Relationship of 18c targets with the nuclear envelope in 36 vertically sectioned amniotic fluid cell nuclei and in 59 horizontally sectioned nuclei, respectively.

^a Number of 18c targets investigated. For definition of 18c target types a-d, see Fig. 2.

^b The percentage of type d in horizontally sectioned nuclei (14.4%) is an upper estimate. Since association of extended 18c targets with both the nuclear envelope was more easily detected in vertically sectioned nuclei (compare Fig. 2), 2.8% would appear to be the more reliable value.

blast nuclei with trisomy X were also used to stain the two Barr bodies representing the two inactivated X chromosomes present in these nuclei (see Fig. 5c). As expected [37] Barr body-CNI distances measured in 240 nuclei showed a significant predominance of larger distances ($P < 0.01$), while 2D distances between the two Barr bodies fit a random model distribution.

Significantly smaller 18c-18c and 18c-CNI 2D distances were confirmed in seven single hybridization experiments using probe L1.84 (Table 2, Nos. 1, 2, 7, 9, 10, 12, and 13). Cell types included normal diploid cells (Table 2, Nos. 1-4, 7, and 8), Bloom's syndrome fibroblasts (Table 2, Nos. 9 and 10) and fibroblasts with trisomy 18 (Table 2, Nos. 12 and 13; Fig. 5a). In spite of considerable variations in the protocols used to prepare the cells for *in situ* hybridization, the same deviation from a random model distribution was obtained in these cell types. In one case (Table 2, No. 13) pretreatment even included a hypotonic shock. Although the mean 2D

TABLE 1B

Combination of the Two 18c Target Types in 59 Horizontally Sectioned Amniotic Fluid Cell Nuclei

	<i>a</i>	<i>b</i>	<i>c</i>	<i>d</i>
<i>a</i>	11	-	-	-
<i>b</i>	19	11	-	-
<i>c</i>	3	4	1	-
<i>d</i>	2	1	0	7

Note. Observed correlations of the two 18c target types a-d (see Fig. 2 for definitions) in 59 horizontally sectioned amniotic fluid cell nuclei.

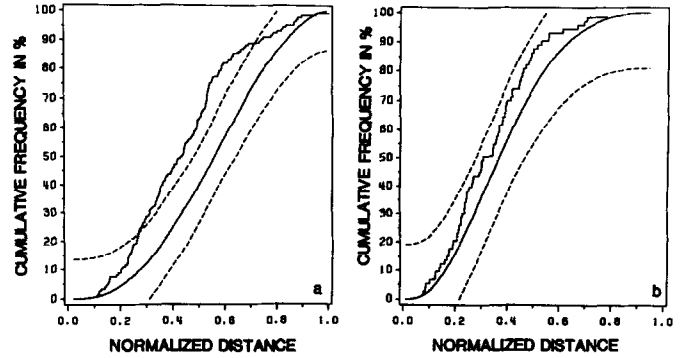


FIG. 3. (a) 3D evaluation of 18c-CN distances (CN, center of the nucleus) and (b) 18c-18c distances performed in 73 3D-reconstructed amniotic fluid cell nuclei after horizontal serial sections with the CSLM. (Abscissa) Normalized 3D distances. (Ordinate) Percentage of nuclei with a normalized 3D distance equal to or smaller than the corresponding distance shown on the abscissa. The smooth curve represents random 3D distances calculated for 10,000 model nuclei of the cylinder model. The hatched lines show the 99% confidence limits ("borderlines") of the one-sample Kolmogorov-Smirnov test. The stepped experimental curve crosses the left borderline in (a), indicating significantly smaller ($P < 0.01$) 18c-CN 3D distances.

area of the nuclei in this experiment was 2.5 times larger than the area of nuclei from the same culture not exposed to hypotonic shock, the ratios of the *x/y* axes were still very similar (Table 2, compare No. 12 with No. 13) indicating that the two-dimensional nuclear configuration was maintained in general.

For each cell type the distributions of 18c and Xc targets were compared by the Kolmogorov-Smirnov two-sample test. All possible comparisons of the experimental curves (except for Experiment 3 with its exceptional distribution of Xc targets) showed that the distribution of 2D distances obtained for 18c targets was significantly different from the distribution obtained for Xc targets ($P < 0.05$ in one case; $P < 0.001$ in all other cases).

DISCUSSION

Using *in situ* hybridization in combination with 3D and 2D image analysis we have found a statistically significant difference in the distribution of chromosome 18 heterochromatin vs X centric heterochromatin in the interphase nucleus of cultured human cells. In particular, both 3D and 2D analyses showed that 18c targets were distributed significantly closer to the nuclear center than predicted by two random model distributions. This result was consistently obtained after various fixation protocols and in various cultured cell types including cells from healthy male and female individuals and from patients with trisomy 18 or Bloom's syndrome (see below for further discussion of the 3D analysis). In contrast, the 2D distribution of centric heterochromatin of the (active) X-chromosome in male cells appeared ran-

TABLE 2
Summary of 14 2D Analyses Performed with the 18c- and Xc-Specific Probes in Various Cell Types

Exp.	Cell material	Karyotype	Pretreatment	Probe-label/detection	n ^a	x/y ^b	Target-target distance ^c			Target-CNI distance ^c	
							18c-18c	Xc-Xc	18c-Xc	18c-CNI	Xc-CNI
1	Amniotic fluid cells	46, XX	a	L1.84- ³ H/autoradiography	286	0.61 ± 0.11	1	—	—	1	—
2		46, XY	a	L1.84- ³ H/autoradiography	274	0.56 ± 0.07	1	—	—	1	—
3	Fibroblastoid fetal lung cells	46, XX	b	L1.84-Bio/AP; pXBR-Hg/PO	275	0.73 ± 0.12	1	1	1	1	1
4		46, XY	b	L1.84-Bio/AP; pXBR-Hg/PO	268	0.68 ± 0.11	1	—	2	1	2
5	Bloom's syndrome fibroblasts	46, XX	a	pXBR- ³ H/autoradiography	318	0.56 ± 0.10	—	2	—	—	2
6		46, XX	a	pXBR-Bio/PO	300	0.57 ± 0.08	—	2	—	—	2
7	Trisomic fibroblasts	46, XY	b	L1.84-Bio/AP	267	0.65 ± 0.12	1	—	—	1	—
8		46, XY	b	L1.84-Bio/AP; pXBR-Hg/PO	253	0.65 ± 0.11	1	—	2	1	2
9	Trisomic fibroblasts	46, XX	a	L1.84- ³ H/autoradiography	330	0.57 ± 0.10	1	—	—	1	—
10		46, XY	a	L1.84- ³ H/autoradiography	264	0.65 ± 0.09	1	—	—	1	—
11	Trisomic fibroblasts	46, XX	a	pXBR- ³ H/autoradiography	423	0.57 ± 0.13	—	2	—	—	2
12		47, XY + 18	b	L1.84-Bio/PO	272	0.65 ± 0.12	1	—	—	1	—
13	Trisomic fibroblasts	47, XY + 18	c	L1.84-Bio/PO	295	0.64 ± 0.10	1	—	—	1	—
14		47, XXX	b	pXBR-Bio/PO	294	0.64 ± 0.11	—	2	—	—	2

Note. Double *in situ* hybridization with probes L1.84 and pXBR was carried out in Experiments 3, 4, and 8. All other experiments reflect single *in situ* hybridizations with either probe L1.84 (Nos. 1, 2, 7, 9, 10, 12, 13) or probe pXBR (Nos. 5, 6, 11, 14). Pretreatment of cells for *in situ* hybridization was performed as described under Materials and Methods (protocols a-c). The probes were either chemically labeled with biotin (Bio) or mercury (Hg) or radioactively labeled with [³H]dTTP (³H). Detection was carried out accordingly with alkaline phosphatase (AP), peroxidase (PO), or autoradiography.

^a Number of the evaluated nuclei in each experiment.

^b (x/y) Average of the axes proportions of the two main axes x and y (± standard deviation).

^c The numbers given in the columns for target-target and target-CNI distances indicate the ranges for the experimental curves (see Ref. [30]). Range 1 indicates a significant predominance ($P < 0.01$) of smaller 2D distances. Range 2 fits the model expectation of random 2D distances, although minor, nonrandom deviations could not be excluded (see above, Statistical analyses). Range 3 indicates a significant predominance of larger 2D distances, but was not observed in any of these *in situ* hybridization experiments.

dom, while the two inactive X-chromosomes (Barr bodies) in female cells with trisomy X were preferentially distributed at the nuclear edge [37]. Two of three double *in situ* hybridization experiments indicated highly variable arrangements of 18c and Xc targets with respect to each other. In a third experiment 2D distances between these targets were significantly smaller. This finding, however, does not indicate a nonrandom relative arrangement of these nonhomologous targets per se, since it can be explained as a consequence of the exceptional finding that both the 18c and Xc targets were distributed closer to the center of the nuclear image.

The possible biological significance of these results should be discussed with several restrictions in mind. While our study has utilized state-of-the-art methods, both findings of random and nonrandom interphase chromosome dispositions may still be subject to methodological artifacts.

First, although the relative arrangements of interphase chromosome targets after *in situ* hybridization are likely to represent the *in vivo* situation to some extent [16, 29] even in air-dried preparations (see Ref. [30] for further discussion), the question to which extent fine structural details of chromatin distribution can be maintained in the course of these experiments cannot be answered satisfactorily at present.

Second, the resolution of the confocal microscope is of crucial importance. Differences in the resolution along the z-axis compared to those along the x,y-axes result in a systematic distortion. For example, the nuclear envelope association of 18c targets observed in our 3D studies needs further confirmation before definitive conclusions can be drawn. To what extent further improvements of the z-axis resolution may be obtained in a confocal microscope by deconvoluting the data is not yet known [6, 19].

Third, some restrictions were expected a priori in the distribution of real chromosomal targets contained within interphase chromosome domains of various size, shape, and orientation compared with the random distribution of points in model nuclei. Furthermore, the four possible distances which could be measured between the two pairs of nonhomologous targets in double *in situ* hybridization experiments were included in our statistical analyses of 18c-Xc 2D distances, although these measurements were also a priori dependent from each other to some extent. For more rigorous statistical testing, only one of the four nonhomologous target-target distances may be randomly chosen in each experimental and model nucleus.

Although our present conclusions will unlikely be affected by refinements of *in situ* hybridization, confocal

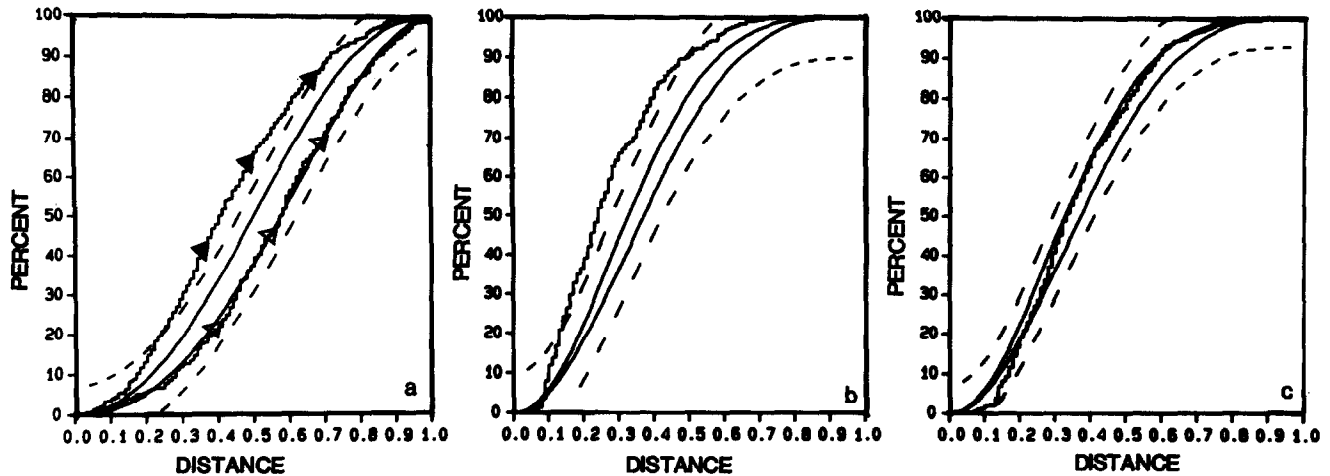


FIG. 4. 2D image analyses of 18c and Xc target distribution after double *in situ* hybridization of amniotic fluid cell nuclei (46, XY) with the biotinylated probe L1.84 (alkaline phosphatase detection) and the mercurated probe pXBR (peroxidase detection) (see Table 2, Experiment 4). (Abscissa) Normalized 2D distances. (a) 18c-CNI distances (black triangles) (CNI, center of the nuclear image); Xc-CNI distances (white triangles), (b) 18c-18c distances, (c) 18c-Xc distances. (Ordinate) Percentage of nuclei ($n = 268$) with a normalized distance equal to or smaller than the corresponding distance on the abscissa. Smooth curves represent random 2D distances calculated for 10,000 model nuclei, i.e., ellipsoids (left smooth curve) and cylinders (right smooth curve). The hatched lines ("borderlines") show the 99% confidence limits of the one-sample Kolmogorov-Smirnov test for the ellipsoid model (left borderline) and for the cylinder model (right borderline). Stepped curves for the experimental 18c-CNI and 18c-18c 2D distances cross the left borderline. This result indicates significantly smaller ($P < 0.01$) mean 2D distances for both the ellipsoid and cylinder model. In contrast, experimental curves for Xc-CNI and 18c-Xc 2D distances are entirely located between the two borderlines, indicating a highly variable and possibly random distribution. The two-sample Kolmogorov-Smirnov test revealed a highly significant difference ($P < 0.001$) between the 18c-CNI distance distribution and the Xc-CNI distance distribution.

microscopy, model calculations, and statistics, such refinements will become essential in future studies using *in situ* hybridization of multiple probes in combination with multicolor techniques [64], in particular in cases where small deviations of experimental data from model calculations must be interpreted. Adequate solutions of

these methodological problems are not easily forthcoming but are of paramount importance for the comprehensive investigation of the chromosomal and suprachromosomal organization of the interphase nucleus.

With these restrictions in mind we shall now discuss possible biological implications of our present results.

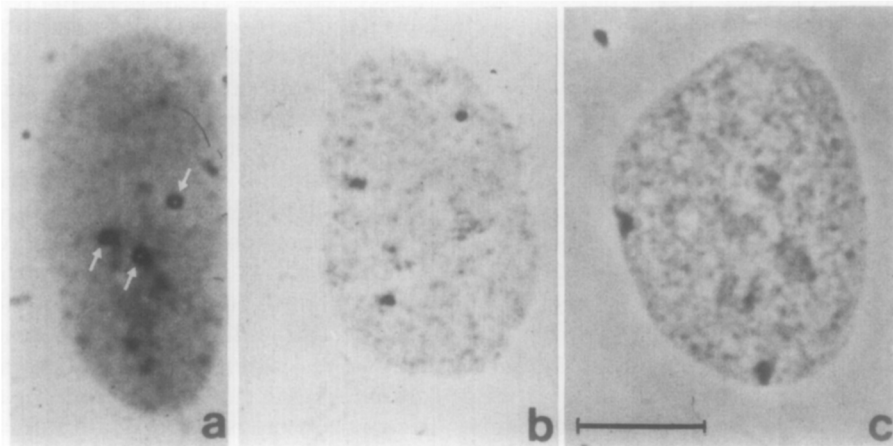


FIG. 5. (a) Nucleus from a trisomic fibroblast cell line (47, XY + 18) hybridized with the biotinylated probe L1.84 (fixation protocol b; peroxidase detection) and counterstained with Giemsa showing three distinct 18c targets (arrows). In addition to their distinct size and shape these targets can be easily distinguished by their dark brown color from blue Giemsa-stained heterochromatin particles. (b) Three distinct Xc targets seen in a nucleus from the fibroblast trisomy X cell line hybridized with the mercurated probe pXBR (fixation protocol b; peroxidase detection). (c) Feulgen-stained nucleus from the trisomy X cell line shows two inactive X chromosomes (Barr bodies). The nucleus was counterstained with nuclear fast red. Bar represents 5 μm .

The nonrandom distribution of 18c appears to be a general phenomenon of the cultured cell types studied so far. Our present and previous studies [30] would fit the hypothesis of a size-dependent distribution of chromosomes in the human interphase nucleus of (some?) mitotically active human cell types as predicted by previous studies of metaphase spreads (see Introduction). Further tests of this hypothesis are under way using chromosome-specific alphoid DNA probes for a variety of other human chromosomes.

The further discussion will be devoted to (a) the problem of homologous chromosome association in somatic cell nuclei and (b) theories of a nonrandom 3D structure of the genome.

(a) The question of whether homologous chromosomes in somatic mammalian cells may be nonrandomly associated with each other has stimulated much controversy [8, 53–56]. This controversy is still far from being settled [12]. We propose to apply the term homologous interphase chromosome association when direct contacts between interphase domains of homologous chromosomes occur significantly more often in a sample of nuclei than can be explained by chance, irrespective of whether these contacts involve nonhomologous or homologous chromosomal subregions. The term *somatic pairing* should be restricted for particularly tight and extended associations of homologous subregions as for example in somatic cells of *D. melanogaster*. When judged by these criteria, our experiments do not support the idea of homologous interphase chromosome association as a general feature of the cell types studied so far in Chinese hamster and man [1, 4, 5, 30, 34, 36, 57]. While 2D distances between Xc targets in four of five experiments fit a random model distribution, our present studies of the 18c distribution provide a case in point that decreased 2D distances between homologous targets *per se* should not be considered as evidence for homologous interphase association. 3D reconstructions showed that the 18c targets in amniotic fluid cell nuclei were preferentially arranged within a nuclear envelope-associated domain near the nuclear center. Associations of the two targets, however, were observed independently from each other with *opposite* sites of the nuclear envelope. Staining of complete interphase domains of chromosomes 18 and X in lymphocytes, amniotic fluid cells, and fibroblasts by the CISS hybridization technique has also demonstrated separation of the homologous domains in most nuclei (Ref. [4] and our unpublished data). On the other hand, Hadlaczky *et al.* [58] have found homologous interphase association of immunostained centromeres in Indian Muntjac cells cultivated *in vitro*. Recently, Arnoldus *et al.* [17] have described the interphase association of the two 1q12 heterochromatic regions in diploid nuclei derived from human cerebellum. In contrast, these regions were variably arranged in nuclei from cere-

bral cortex. These data reinforce the view that the extent of homologous interphase association of specific chromosomes may vary in different cell types.

The possibility has been considered that the increased frequencies of interchanges between homologous chromosomes observed in Bloom's syndrome cells [59] would reflect an increased probability of interphase contacts compared to those of cells from normal persons [60]. In agreement with our findings in normal diploid and trisomic nuclei, our present experiments do not indicate homologous interphase association of 18c and Xc targets in Bloom's syndrome cells. Alternatively, homologous interchanges in Bloom's syndrome cells might be facilitated whenever homologous chromosome regions come into contact with each other by chance [60].

(b) Blobel [61] has put forward the hypothesis that within the global confines of the cell nucleus, expanded and compacted domains of each chromosome were three-dimensionally coordinated with those of other chromosomes to yield a dynamic 3D structure of the genome. This 3D structure should be distinctly different at different stages of the cell cycle and in different cell types of a complex multicellular organism. Previous [1, 4, 5, 30, 34, 36, 40, 41, 57] and present experiments have demonstrated an impressive variability of both homologous and nonhomologous chromosome arrangements in cultivated Chinese hamster and human cells. This apparent variability may indicate that the interphase chromosome arrangements, which we have investigated, were irrelevant with regard to the normal genetic regulation of these cells. Probabilistic differences of 18 and X positioning may simply reflect differences in the physical and chemical properties of these chromosomes and the mechanics of mitosis [6]. Still, any generalization of such findings may be misleading. Cell cycle and cell type-specific differences of the suprachromosomal organization may have been obscured in this study, since *in vitro* cultures represented complex systems of cells in various states of differentiation and cell cycle rather than homogeneous cell populations.

In conclusion, many more experiments must be carried out to resolve these controversies, including more chromosome-specific probes and various normal and pathological cell populations which are well defined both with regard to cell cycle and functional differentiation. Precise three-dimensional chromosomal positioning may be restricted to certain subsets of chromosomes or chromosomal subregions and these nonrandomly arranged subsets may vary in different cell types (see also Introduction). Such a hypothesis would give room for sufficient variability of chromosomal arrangements to account for both the observation that balanced chromosomal translocations are often tolerated in individuals without adverse effects and the profound reshuffling of chromosome material which has taken place during evo-

lution [62]. If a functionally important, dynamic 3D structure of the genome turns out to be more than a *fata morgana* of the human mind, such evolutionary reshuffling should keep intact those syntenic regions whose chromosomal and/or suprachromosomal 3D topography were of crucial importance for the functioning of certain cell types. In addition, such reshuffling may have placed new restrictions on the possible 3D structures of a genome and thus have played a role in the evolution of species. Whatever the answers to the questions raised above may be, we consider such studies to be an indispensable part of any effort to improve our understanding of the functioning of genomes above the level of individual genes. The methods now available should make it possible to settle such questions convincingly.

We thank Dr. J. S. Heslop-Harrison (University of Cambridge, UK) for helpful discussions, Dr. H. D. Hager (University of Heidelberg, FRG) and Professor Dr. H. W. Rüdiger (University of Hamburg, FRG) for providing cell cultures, Dipl. Phys. C. Storz (EMBL Heidelberg, FRG) for help in the use of the CBSLM, Mrs. A. Wiegenstein for photographic work, and the German Cancer Research Center (Heidelberg, FRG) for use of a VAX 11-780. T. Cremer was supported by a Heisenberg-Stipendium of the Deutsche Forschungsgemeinschaft.

REFERENCES

- Cremer, T., Cremer, C., Baumann, H., Luedtke, E. K., Sperling, K., Teuber, V., and Zorn, C. (1982a) *Hum. Genet.* **60**, 46-56.
- Schardin, M., Cremer, T., Hager, H. D., and Lang, M. (1985) *Hum. Genet.* **71**, 281-287.
- Manuelidis, L. (1985) *Hum. Genet.* **71**, 288-293.
- Lichter, P., Cremer, T., Borden, J., Manuelidis, L., and Ward, D. C. (1988a) *Hum. Genet.* **80**, 224-234.
- Cremer, T., Lichter, P., Borden, J., Ward, D. C., and Manuelidis, L. (1988b) *Hum. Genet.* **80**, 235-246.
- Mathog, D., and Sedat, J. W. (1989) *Genetics* **121**, 293-311.
- Schwarzacher, T., Leitch, A. R., Bennett, M. D., and Heslop-Harrison, J. S. (1989) *Ann. Bot.* **64**, 315-324.
- Comings, D. E. (1980) *Hum. Genet.* **53**, 131-143.
- Bennett, M. D. (1982) in *Genome Evolution* (Dover, G. A., and Flavell, R. B., Eds.), pp. 239-261, Academic Press, London.
- Hubert, M., and Bourgeois, C. A. (1986) *Hum. Genet.* **74**, 1-15.
- Cremer, T., Emmerich, P., and Lichter, P. (1987) *Ann. Univ. Sarav. Med. Suppl.* **7**, 67-71.
- Hilliker, A. J., and Appels, R. (1989) *Exp. Cell Res.* **185**, 297-318.
- Schmid, M., and Krone, W. (1976) *Chromosoma* **56**, 327-347.
- Manuelidis, L. (1984) *Proc. Natl. Acad. Sci. USA* **81**, 3123-3127.
- Brinkley, B. R., Brenner, S. L., Hall, J. M., Tousson, A., Balczon, R. D., and Valdivia, M. M. (1986) *Chromosoma* **94**, 309-317.
- Borden, J., and Manuelidis, M. (1988) *Science* **242**, 1687-1691.
- Arnoldus, E. P. J., Peters, A. C. B., Bots, G. T. A. M., Raap, A. K., and van der Ploeg, M. (1989) *Hum. Genet.* **83**, 231-234.
- Guttenbach, M., Schmid, M., Jauch, A., and Vogt, P. (1989) *Chromosoma* **97**, 429-433.
- Agard, D. A., and Sedat, J. W. (1983) *Nature (London)* **302**, 676-681.
- Rawlins, D. J., and Shaw, P. J. (1988) *J. Cell Sci.* **91**, 401-414.
- Oud, J. L., Mans, A., Brakenhoff, G. J., van der Voort, H. T. M., van Spronsen, E. A., and Nanninga, N. (1989) *J. Cell Sci.* **92**, 329-339.
- Jovin, T. M., and Arndt-Jovin, D. J. (1989) *Annu. Rev. Biophys. Biophys. Chem.* **18**, 271-308.
- Manuelidis, L., Langer-Safer, P. R., and Ward, D. C. (1982) *J. Cell Biol.* **95**, 619-625.
- Rappold, G. A., Cremer, T., Cremer, C., Back, W., Bogenberger, J., and Cooke, H. J. (1984a) *Hum. Genet.* **65**, 257-261.
- Landegent, J. E., Jansen de Wal, N., Baan, R. A., Hoeijmakers, J. H. J., and van der Ploeg, M. (1984) *Exp. Cell Res.* **153**, 61-72.
- Hopman, A. H. N., Wiegant, J., and van Duijn, P. (1987) *Exp. Cell Res.* **169**, 357-368.
- Lichter, P., Cremer, T., Chang Tang, C. J., Watkins, P. C., Manuelidis, L., and Ward, D. C. (1988b) *Proc. Natl. Acad. Sci. USA* **85**, 9664-9668.
- Pinkel, D., Landegent, J., Collins, C., Fuscoe, J., Segraves, R., Lucas, J., and Gray, J. W. (1988) *Proc. Natl. Acad. Sci. USA* **85**, 9138-9142.
- Manuelidis, L., and Borden, J. (1988) *Chromosoma* **96**, 397-410.
- Emmerich, P., Loos, P., Jauch, A., Hopman, A. H. N., Wiegant, J., Higgins, M., White, B. N., van der Ploeg, M., Cremer, C., and Cremer, T. (1989) *Exp. Cell Res.* **181**, 126-140.
- Brakenhoff, G. J., Blom, P., and Barends, P. (1979) *J. Microsc.* **117**, 219-232.
- Cremer, C., and Cremer, T. (1978) *Microsc. Acta* **81**(1), 31-44.
- Wijnaendts-van-Resandt, R. W., Marsman, H. J. B., Kaplan, R., Davoust, J., Stelzer, E. H. K., and Stricker, R. (1985) *J. Microsc.* **138**, 29-34.
- Rappold, G. A., Cremer, T., Hager, H. D., Davies, K. E., Müller, C. R., and Yang, T. (1984b) *Hum. Genet.* **67**, 317-325.
- Cremer, T., Landegent, J., Brückner, A., Scholl, H. P., Schardin, M., Hager, H. D., Devilee, P., Pearson, P., and van der Ploeg, M. (1986) *Hum. Genet.* **74**, 346-352.
- Cremer, T., Tesin, D., Hopman, A. H. N., and Manuelidis, L. (1988a) *Exp. Cell Res.* **176**, 199-220.
- Belmont, A. S., Bignone, F., and Ts'o, P. O. P. (1986) *Exp. Cell Res.* **165**, 165-179.
- Hens, L., Kirsch-Volders, M., Verschaeve, L., and Susanne, C. (1982) *Hum. Genet.* **60**, 249-256.
- Wollenberg, C., Kiefaber, M. P., and Zang, K. D. (1982) *Hum. Genet.* **62**, 310-315.
- Cremer, T., Baumann, H., Nakanishi, K., and Cremer, C. (1984) in *Chromosomes Today* (Bennett, M. D., Gropp, A., and Wolf, U., Eds.), Vol. 8, pp. 203-212, Allen & Unwin, London.
- Baumann, H. (1983) Thesis, University of Heidelberg.
- Ochs, B., Franke, W. W., Moll, R., Grund, C., Cremer, M., and Cremer, T. (1983) *Differentiation* **24**, 153-173.
- Hayflick, L. (1965) *Exp. Cell Res.* **37**, 614-636.
- Yang, T. P., Hansen, S. K., Oishi, K. K., Ryder, O. A., and Hamkalo, B. A. (1982) *Proc. Natl. Acad. Sci. USA* **79**, 6593-6597.
- Devilee, P., Cremer, T., Slagboom, P., Bakker, E., Scholl, H. P., Hager, H. D., Stevenson, A. F. G., Cornelisse, G. J., and Pearson, P. L. (1986a) *Cytogenet. Cell Genet.* **41**, 193-201.
- Devilee, P., Slagboom, P., Cornelisse, C. J., and Pearson, P. L. (1986b) *Nucleic Acids Res.* **14**, 2059-2073.

47. Langer, P. R., Waldrop, A. A., and Ward, D. C. (1981) *Proc. Natl. Acad. Sci. USA* **78**, 6633-6637.
48. Hopman, A. H. N., Wiegant, J., and van Duijn, P. (1986) *Histochemistry* **84**, 169-178.
49. Johnson, G. D., and de C. Nogueira Araujo, G. M. (1981) *J. Immunol. Methods* **43**, 349-350.
50. Schwarzacher, H. G. (1970) in *Methoden in der medizinischen Cytogenetik* (Schwarzacher, H. G., and Wolf, U., Eds.), pp. 150-171, Springer-Verlag, Berlin.
51. Stelzer, E. H. K., Stricker, R., Pick, R., Storz, C., and Hänninen, P. (1989) *SPIE Proc.* **1028**, 146-151.
52. Sachs, L. (1968) *Angewandte Statistik*. Springer-Verlag, Berlin.
53. Comings, D. E. (1968) *Amer. J. Hum. Genet.* **20**, 440-460.
54. Vogel, F., and Schroeder, T. M. (1974) *Humangenetik* **25**, 265-297.
55. Avivi, L., and Feldman, M. (1980) *Hum. Genet.* **55**, 281-295.
56. Heslop-Harrison, J. S., Smith, J. B., and Bennett, M. D. (1988) *Chromosoma* **96**, 119-131.
57. Cremer, T., Cremer, C., Schneider, T., Baumann, H., Hens, L., and Kirsch-Volders, M. (1982b) *Hum. Genet.* **62**, 201-209.
58. Hadlaczky, G. Y., Went, M., and Ringertz, N. R. (1986) *Exp. Cell Res.* **167**, 1-15.
59. Schroeder, T. M., and German, J. (1974) *Humangenetik* **25**, 299-306.
60. Kuhn, E. M. (1981) *Hum. Genet.* **58**, 417-421.
61. Blobel, G. (1985) *Proc. Natl. Acad. Sci. USA* **82**, 8527-8529.
62. O'Brien, S. J., and Seuanez, H. N. (1988) *Annu. Rev. Genet.* **22**, 323-351.
63. Rosa, P., Weiss, U., Pepperkok, R., Ansorge, A., Niehrs, C., Stelzer, E. H. K., and Huttner, W. B. (1989) *J. Cell Biol.* **109**, 17-34.
64. Nederlof, P. M., Robinson, D., Abuknesha, R., Wiegant, J., Hopman, A. H. N., Tanke, H. J., and Raap, A. K. (1989) *Cytometry* **10**, 10-27.

Received November 6, 1989

Revised version received January 29, 1990